

Factors affecting the interfacial adsorption of stabilisers on to titanium dioxide particles (flow microcalorimetry, modelling, oxidation and FTIR studies): Nano versus pigmentary grades

Norman S. Allen^{a,*}, Michele Edge^a, Amaya Ortega^a, Christopher M. Liauw^a,
John Stratton^b, Robert B. McIntyre^b

^a *Department of Chemistry and Materials, Faculty of Science and Engineering, The Manchester Metropolitan University, Chester Street, Manchester M1 5GD, UK*

^b *Millenium Inorganic Chemicals, PO Box 26, Grimsby, N.E. Lincs, DN41 8DP, UK*

Received 19 May 2005; accepted 25 May 2005

Available online 25 July 2005

Abstract

A series of nano and micron particle size anatase and rutile titanium dioxide (TiO₂) were prepared with various densities of surface treatments in order to examine the influence of the particle size on the photoactivity of the titania particle surface and their degree and nature of interfacial interaction with polymer stabilisers namely, Irganox 1010 (Phenolic type) and Tinuvin 770 (hindered piperidine type). The surface characteristics of the synthesized powders were studied by Diffuse Reflectance Fourier Transform Infrared Spectroscopy (DRIFTS). The surface area was determined using the Brunauer Emmett Teller (N₂ BET) method, and particle size measurements using X-ray diffraction (XRD) and transmission electron microscopy (TEM). The photochemical activities of the titania particles have been examined by monitoring the oxygen consumption during photo-oxidation of 2-propanol. Surface activity of the titania with stabilisers has also been examined by flow microcalorimetry (FMC) and DRIFTS in order to determine the nature of the interfacial interactions with different polymer stabilisers. Photoactivity assessment verified the higher activity of the nanoparticles. Hydroxyl groups were also found to be accountable for the higher photoactivity of the nanoparticles. The rutile crystal form conferred an inherent photostabilising effect that was further improved by surface coating with alumina. FMC studies revealed that the calcination of nanoanatase increased adsorption activity of hindered phenol and hindered amine probes, with the latter being more strongly adsorbed due to the higher basicity of the amine functionality. DRIFTS indicated adsorption may also occur through the ester functionalities. Calcination of the titania causes a reduction in the surface concentration of Ti–OH and hence a reduction in the amount of strongly adsorbed water blocking the adsorption sites and possibly bridging the amorphous primary particles on the uncalcined sample. With the calcined samples the adsorption activity was proportional to surface area. The physical and chemical nature of these intermolecular forces are assessed and discussed in relation to the potential effects on polymer stabilisation processes.

© 2005 Elsevier Ltd. All rights reserved.

Keywords: Titanium dioxide; Pigments; Nanoparticles; Degradation; Oxidation; Microcalorimetry; Interfacial adsorption

* Corresponding author. Tel.: +44 161 247 1432; fax: +44 161 247 6357.
E-mail address: n.s.allen@mmu.ac.uk (N.S. Allen).

1. Introduction

The effect of titanium dioxide surface chemistry on interfacial interactions with stabilisers has not been studied in detail. In thermoplastics, the adsorption of stabilisers onto fillers is a recognised problem that is solved by using additives which sacrificially adsorb on to the filler surfaces thereby blocking the adsorption of the stabilisers [1]. Previous studies on silicas for example, indicated that the adsorption of stabilisers is not necessarily a negative feature and this can be used to provide what can be considered as a reservoir of stabilisers for controlled activity [2]. In order to understand how stabilisers are adsorbed and under which conditions they can be released, the interactions between pigments (fillers) and polymer additives must be well understood. Flow microcalorimetry (FMC) has proved to be a useful technique for studying such interactions and has become an established method for characterising filler surfaces in terms of their surface chemistry and their interactions with surface treatments etc. The technique was initially used for this purpose by Fowkes [3] and later refined by Ashton and Briggs [4]. FMC enables heats of adsorption and desorption to be measured and, with added concentration detectors, amounts adsorbed/desorbed can be obtained. The latter enables calculation of molar heats of adsorption–desorption. Knowledge of the microstructure of pigments and fillers is of great importance in understanding what processes limit the efficiency of the powders. It is important to recognise that the bulk properties of the materials such as mechanical, electronic and optical properties depend on the atomic and molecular structure of the materials.

The science of ultrafine particles on a nanometric scale has attracted considerable attention in recent years. Varieties of techniques and characterisation tools have been developed to prepare and study these particles. A unique property of nanoparticles is their extremely high surface area: they have many more sites for achieving property enhancements, making them ideal for a wide variety of applications. In recent years extensive studies have been undertaken on characterising interfacial interactions on carbon black particles of varying manufacturing types and polymer stabilisers [5–7] as an example. Here the nature of surface functional groups on the carbon blacks and acid–base characteristics were thoroughly characterised and measured. Both stabiliser adsorption and desorption properties were also measured and related in many cases to their interactive performance in the polymer during thermal and photo-oxidation processes. The presence of impurities such as sulphur compounds and adsorbed water were also found to cause further complications in the surface analysis of carbon black and so influence the adsorption properties of the stabilisers and their performance. Similar studies have also been undertaken on silica fillers [2].

Presently there is a rapidly growing interest in nanoscale TiO₂ materials in research activities. Catalysis by TiO₂ has become a very active field of research and it can be designed with a high efficacy by combining the physical properties of TiO₂ as a photocatalytic semiconductor and/or by doping the TiO₂ with various transition metal oxide systems. On the other hand the absorption of UV light by TiO₂ may be utilised for solar radiation panels. In all these applications, the morphology, average particle size and size distribution, phase composition and porosity of titania powders are important factors to be controlled. Nanoparticles show a great tendency to aggregate due to high surface energy combined with their high surface area to volume ratio. This aggregation tendency impedes their use in a variety of applications. For these reasons the synthesis of ultrafine particles with controlled size and surface chemistry is of technological interest.

In recent work we examined the role of uncoated ultrafine titanium dioxide pigments in alkyd and acrylic based paint films [8,9]. This work highlighted a very clear difference in behaviour between nanoparticle and pigmentary grade titanium dioxide with the former being more active in its uncoated form. Surface modifications of the TiO₂ particles with inorganic hydrates were found to reduce the photochemical reactivity of titanium pigments. This can reduce the generation of free radicals by physically inhibiting the diffusion of oxygen and preventing release of free radicals. The photosensitivity of titanium dioxide is considered to arise from localized sites on the crystal surface, and occupation of these sites by surface treatments inhibits photo-reduction of the pigment by ultraviolet radiation and hence the destructive oxidation of the binder is inhibited. However, because such pigment particles are so small, their specific surface area is very high and therefore, important to the pigment's chemical performance. Thus, surface characteristics have profound impact on interactions of pigments with all the other components of polymer materials on the substrate. Titanium dioxide particles on the surface contain both basic terminal and acidic bridged-hydroxyl groups and these may be associated with the titania or a hydrous oxide coating. It will also possess labile Ti–O–Ti bonds, water molecules adsorbed at Lewis acid sites or surface hydroxyl groups as well as adsorbed anions such as sulphate and chloride process residues. All these species can exhibit strong interactions with polymer additives, in particular stabilisers, causing often antagonistic effects as reported recently [8,9]. Thus, hindered piperidine light stabilisers being basic in character have been found to exhibit little stabilisation effect in the presence of photocatalytic grade anatase nanoparticles.

This study aims to correlate the surface properties and particle size with the interfacial interactions of a range of pigmentary and nanoparticle titania pigments

with two stabilisers of the structures shown in Table 1 using the technique of flow microcalorimetry (FMC). In the first instance the surface of the pigment powders have been characterised by Fourier Transform Infrared Spectroscopy (DRIFTS). Secondly, we have attempted to determine the surface area and size of the TiO₂ crystallites and particle size distribution in a polymer media by different techniques such as Brunauer Emmett Teller (BET) method and X-ray diffraction (XRD). The photoactivity of the pigments has been assessed rapidly by using an isopropanol oxidation test and correlated with surface hydroxyl analysis. By choosing a phenolic antioxidant and a hindered piperidine light stabiliser (Table 1) potential surface interactions can be ascertained and interfacial processes more clearly understood in terms of the effects on polymeric systems. Molecular modelling has also been undertaken to assist in the interpretations.

2. Experimental

2.1. Materials

The titanium dioxide pigments were all experimental grades prepared in the laboratories of Millennium Chemical Company, Grimsby, UK. The pigments codes and characteristics are given in Tables 2 and 3, respectively.

Nanoparticles were prepared by the sulphate process. The titanyl sulphate formed was hydrolysed and the precipitate formed was used for preparing the anatase nanoparticle and normal size pigments. The precipitate obtained was washed and dried to obtain pigment A. Pigments B, C and D were calcined at increasing temperatures 500, 600, and 900 °C, respectively, to promote crystal growth producing different crystallite sizes.

Rutile pigments were prepared by the chloride route. Increasing levels of inorganic treatment and also an organic treatment were applied to the surface of the rutile pigments producing pigments E, F and G.

The stabilisers used were: a hindered piperidine light stabiliser Tinuvin 770 and a primary hindered phenolic antioxidant, Irganox 1010. Structures and further details are given in Table 1.

2.2. Methods

2.2.1. Diffuse reflectance Fourier transform infrared spectroscopy (DRIFTS)

TiO₂ samples (5% w/w) were mixed using a gentle folding action with finely ground KBr at 5% and analysed using a NICOLET 510P FTIR spectrophotometer fitted with a Spectra-Tech DRIFTS cell. Control, data recording and analysis were performed using a PC running Nicolet software. The spectra were obtained from 164 scans and the resolution was 4 cm⁻¹.

2.2.2. Isopropanol oxidation test

Photocatalytic activity measurements were conducted using a gas phase unit. IPA (isopropyl alcohol) was used as a reactant in the presence of air. Oxygen consumption was measured before and after UV exposure in a sealed glass tube and is representative of photocatalytic activity.

Titanium dioxide was loaded as a powder on a metallic (stainless steel) support. Three 8-W black light (maximum peak 340 nm) bulbs were used. The oven temperature was 40 °C. A 5 h exposure time was used. Results are expressed as % oxygen consumption after 5 h of exposure.

2.2.3. Flow microcalorimetry

Flow microcalorimetry (FMC) was used to investigate the interactions between the titanium dioxides and

Table 1
Structures of stabilisers

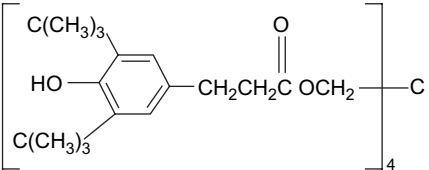
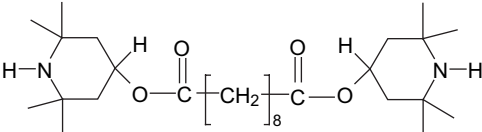
Trade name, nomenclature	Molar mass	Chemical structures, supplier
Irganox 1010, tetrakis[methylene-3-(3',5'-di-tertbutyl-4-hydroxyphenyl)propionate]methane	1178	 <p>Ciba Specialty Chemicals</p>
Tinuvin 770, bis(2,2,6,6-tetramethyl-4-piperidyl)sebacate	481	 <p>Ciba Specialty Chemicals</p>

Table 2
Properties of titanium dioxide pigments

Sample	Crystalline form	Preparation process	Sulphate SO ₂ (%)	Alumina Al ₂ O ₃ (%)	Organic treatment
A	Nanoanatase	Sulphate	<0.8		
B	Nanoanatase	Sulphate	<0.8		
C	Nanoanatase	Sulphate	<0.8		
D	Anatase	Sulphate			
E	Rutile	Chloride		1	Yes
F	Rutile	Chloride		2.8	Yes
G	Rutile	Chloride		3.4	Yes

a primary hindered phenolic antioxidant, Irganox 1010, and a hindered amine light stabiliser, Tinuvin 770 (Table 1). Adsorption and desorption of any molecule onto a surface involves a change in enthalpy. FMC measures this change of enthalpy when the experiment is carried out under flow conditions. Here a differential refractometer connected to the cell outlet allows the quantification of probe adsorbed on the titanium dioxide surface.

The FMC consists of a Microscal 3Vi connected to Waters 410 differential refractometer. The resulting data were output to a Perkin Elmer Nelson 970 series data station and analysed using a Perkin Elmer Turbochrom version 4-chromatography software. The scheme of the system is shown in Fig. 1. The basic experimental conditions were conducted using a cell temperature of 25 °C (± 1 °C). The filler is placed inside the calorimeter cell (0.15 cm³). Solvent (*n*-heptane, Aldrich HPCL grade) is run through it for about an hour allowing the filler to reach equilibrium with the solvent. Then a solution of known concentration of the probe (0.2% w/w) is run through the cell. The solvent flow rate was 5 ml h⁻¹. The calorimeter measures the enthalpy change that occurs when a probe molecule displaces a solvent molecule from an adsorption site on a TiO₂ surface. On switching the cell in let back to pure solvent, the enthalpy change that occurs when a solvent molecule displaces a probe molecule can also be measured.

As the solution is passed through the filler, the probe adsorbs on to its surface. The heat of adsorption

causes an increase in temperature, which is detected by thermistors and registered by the ADC PC interface. Desorption will cause a decrease in temperature, which will also be registered. These results are plotted as millivolts against time. The heat of adsorption/desorption can be determined using a calibration constant generated by inputting a known amount of electric power into a resistance wire filament that is integrated into the outlet connector (see Fig. 1). The area under the peaks can thus be transformed into heat change, and therefore the heat of adsorption/desorption is related to the surface area of the filler or the molar amount of probe. All solvents used were of “analar” quality and obtained from the Aldrich Chemical Company, Gillingham, UK.

The amount of probe adsorbed is determined by measuring the concentration of probe in the cell effluent as a function of time. In this investigation this was achieved using a differential refractometer. Typical data are shown in Fig. 2; after all the adsorption sites on the filler surface become occupied by solvent molecules and possible formation of multilayers, the differential refractometer (DR) response reaches a limiting value. In the case of a specially chosen non-adsorbing probe the limiting value in DR response is attained much more rapidly (Fig. 3). The amount of probe adsorbed is determined by normalising the overall non-adsorbing probe DR response to that of the probe DR response. The non-adsorbing data are then subtracted from that of the probe. The resulting negative peak is proportional to the amount of probe adsorbed. Calibration is performed by injecting a known volume of probe solution from the calibration loop (20 μ l) into a flow of solvent that goes through the refractometer. The detector produces a peak for each of the injections and the average of the area of these peaks is used to obtain the amount adsorbed/desorbed onto/from the filler.

2.2.4. Molecular modelling

The structures of the stabilisers used in this study have been modelled using AccuModel (Version 1.1) for stick and CPK (Corey–Pauling–Culpen) models.

3. Results and discussion

3.1. Photoactivity of Titania

This photoactivity of the titania particles has been ascertained via the 2-propanol oxidation test. The oxidation of propan-2-ol to yield acetone is a specific methodology and in this study is related to oxygen consumption during irradiation of the medium in the presence of the titania pigments. Thus the rate of acetone formation is said to relate directly to the reactivity of the particular TiO₂ pigment, therefore offering a good prediction of the photoactivity of the pigment.

Table 3
BET surface area and particle size for titania pigments

Sample	BET surface area (m ² g ⁻¹)	Particle size (nm) (calculated assuming no porosity)
Pigment A	329.1	4.3
Pigment B	77.9	18.3
Pigment C	44.4	32.2
Pigment D	10.1	140
Pigment E	6.4	220
Pigment F	12.5	110
Pigment G	12.5	110

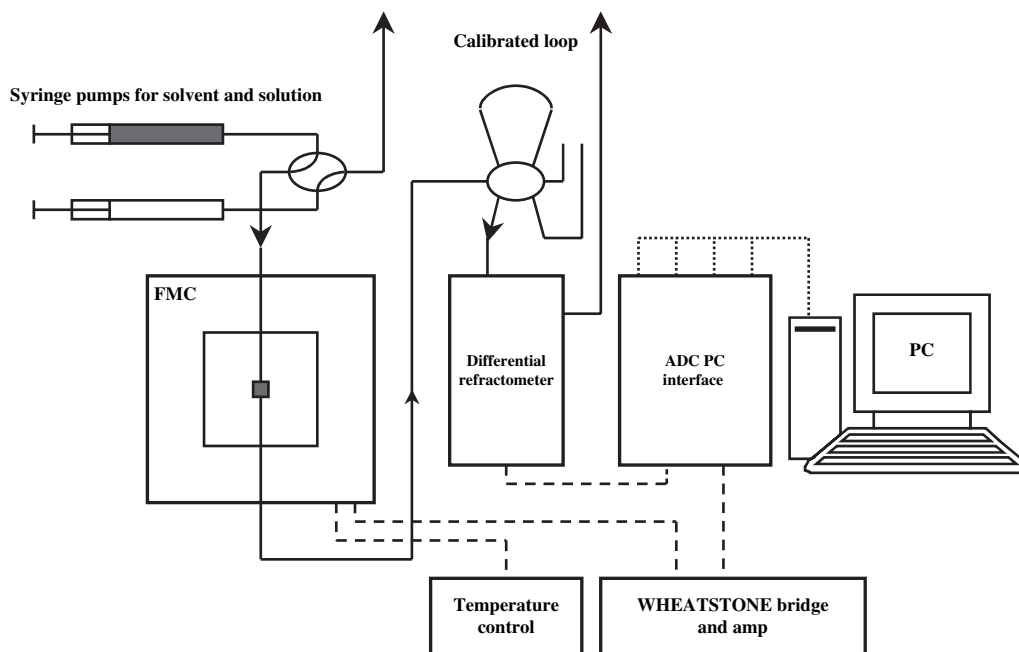


Fig. 1. Schematic diagram of flow microcalorimetry.

It is likely that many factors account for the differences in photoactivity between the samples. However, it is immediately apparent that particle size plays a significant role. As the surface area increases the number of surface hydroxyls will also increase and as shown later these are of prime importance with respect to photoactivity. Broonstra and Mutsears [10] found a linear relationship between the surface concentration of hydroxyls and the amount of oxygen adsorbed. They stated that when hydroxyls were displaced photoadsorption of oxygen decreased.

The data for both tests are compared in Table 4. There are a number of correlations and trends within the data. Firstly, the content of hydroxyl groups corresponds to that of the photoadsorption of oxygen after 5 h of exposure time. In general, an increase in the hydroxyl content showed a higher adsorption of oxygen adsorbed.

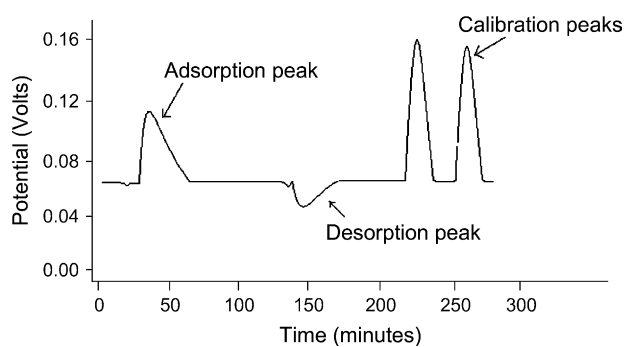


Fig. 2. FMC adsorption, desorption and calibration energy peaks in function of time for the adsorbing probe.

Secondly, all the nanoparticulate grades exhibit higher photoactivity than the pigmentary grades. Pigment A shows the higher hydroxyl content followed by pigments B and C. This can be observed in the FTIR results where a greater amount of physisorbed water is retained in the crystal lattice of pigment A; this physisorbed water is likely to be associated with hydroxyl groups. Additionally, it has been reported that calcination also reduces the number of OH groups on the surface of the photocatalyst, leading to an overall reduction in the photoactivity catalyst [11]. This is observed in Fig. 4, which shows the variation of BET surface area and OH content as a function of calcination temperature of TiO_2 . A decrease in the surface area and OH content with increasing calcination temperature is observed.

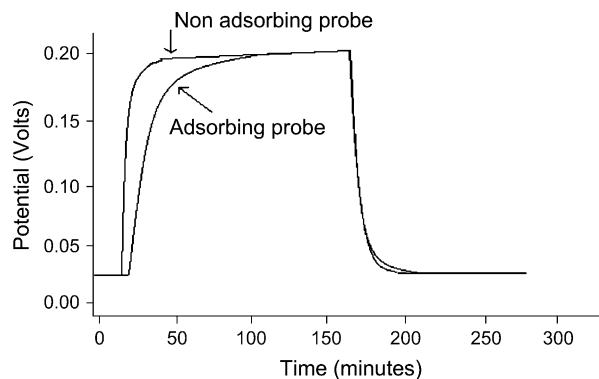


Fig. 3. Differential refractometer response as a function of time for the non-adsorbing and adsorbing probe.

Table 4
Relationship between photoactivity measured by oxidation of propan-2-ol and hydroxyl content of titanium dioxide pigments

Pigment	OH Content (mmol g ⁻¹)	Oxygen consumption (%)
A	0.78	4.3
B	0.53	5.2
C	0.32	3.8
D	0.05	1.4
E	0.02	0.3
F	0.05	1.4
G	—	1.1
2-Propanol control	—	0.2

However, the order of photoactivity for nanoparticles is not in concordance with the surface area/particle size. Nanoparticle B shows higher oxygen consumption compared with nanoparticle A. The photocatalytic properties of the different pigments show significant differences, which must be due to differences in bulk or surface properties. The bulk properties determine the processes of charge carrier photogeneration and diffusion, whereas those of the surface influence both the adsorption of organic molecule and the generation of species necessary for photoreaction [12]. Regarding the bulk properties of the pigment, the photocatalytic activity depends on the ratio of the photo-generated surface carriers transfer rate to the electron hole recombination. The increased photocatalytic activity of nanoparticles can be attributed to their particle size.

Firstly, according to Wang and co-workers [13] the average diffusion time is proportional to the particle size. As such, the smaller particle size contributes to a shorter diffusion time for the photo-generated carriers to reach the surface from the interior of the particle. In addition, published studies have shown that electrons and holes are trapped very quickly [14].

$$t = \frac{r}{\pi^2 D} \quad (1)$$

where

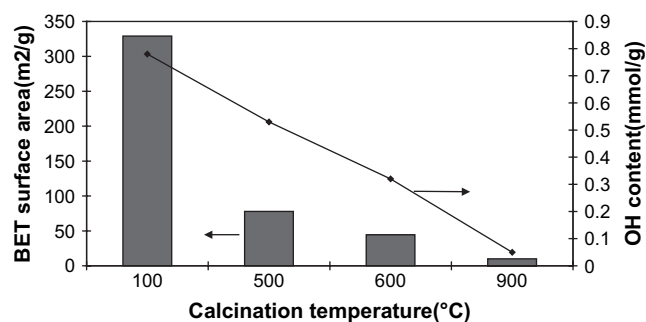


Fig. 4. Variation of the BET surface area (m² g⁻¹) and OH content (mmol g⁻¹) as a function of the calcinations temperature (°C).

t represents the average diffusing time;
 r represents the grain size; and
 D represents the diffusing coefficient of carriers.

Therefore, a small particle size can enhance separation efficiency and reduce the combination efficiency of the photo-generated electric charge. The differences in the values for both nanoparticles A and B may be caused in part by a greater internal porosity of sample A (as found in our analysis by TEM). The decrease in the photoactivity of this pigment can be attributed to the structural and electronic defects which can capture the electrons and holes produced by irradiation before they reach the surface of the pigment.

The infrared spectroscopic analysis of the TiO₂ samples showed that the surface hydroxyl concentration of nanoparticles is highest, this feature not only favours the trapping of electrons that enhance the separation efficiency of the electron–hole pair, but also favours the formation of hydroxyl radicals.

In addition, the difference in the photoactivity of nanoparticle A could be due in part to its morphology. TEM analysis showed the pigment A morphology comprising an agglomeration of small primary crystallites (a few nanometres in size) thus creating a small porous structure. The isopropanol molecule may not be able to penetrate these pores, and hence the full N₂ BET surface area is not accessible to the molecule.

Thus, in comparison, the structure of nanoparticle B provides greater external surface sites. The availability of the surface allows greater exposure and contact between the catalyst, light and substrates and therefore it is more beneficial for photoreaction.

The pigmentary (micron scale) anatase particles (sample D) are more active than the rutile types (Samples F and G) the latter being the least active and most durable pigment due to its higher level of surface treatment. Apart from the particle size, the crystal structure and surface treatment have an important role in the photoactivity of the pigment.

3.2. Interfacial characteristics of pigments

Problems associated with adsorption of stabilising additives onto high surface area fillers such as titanium dioxide are well known in the industry. Adsorption of certain antioxidants and light stabilisers onto the surface of titanium dioxide can prevent them from protecting the polymer and hence severely compromises the heat and light stability of the matrix [8,9]. The stabilisers used in this study were Irganox 1010 and Tinuvin 770 (Table 1) that have previously been used in polymer degradation studies in order to compare the activity of different titanium dioxide pigments. FMC allows the measurement of the energy involved in the processes of adsorption and desorption and the calculation of the amount of each

compound adsorbed or desorbed on or from the titanium dioxide surface.

3.3. Adsorption of Tinuvin 770

Adsorption and desorption energies resulting from the interactions of the hindered amine light stabiliser, Tinuvin 770, with the titanium dioxide pigments are shown in Fig. 5. The enthalpies of adsorption are exothermic but the values have been converted to a positive value to ease the representation.

Firstly, it can be observed that the energy released during adsorption is greater than that required for desorption. Hence, more molecules are strongly adsorbed than desorbed. The first molecules to be adsorbed will interact with the most energetic adsorption sites. The first molecules to be desorbed will be those bound to the weakest sites, causing the average heat to be larger for adsorption than for desorption.

Nanosized anatase, B and C, and micron sized anatase pigmentary (D) showed more adsorption than anatase nanoparticle A and rutile pigmentary grades E, F and G. This implies that the particle size and BET surface area are not the only major factors affecting the adsorption processes.

Fig. 6 compares the amount of Tinuvin 770 adsorbed for the different titanium dioxide pigments. Interesting results were observed from these data. Differences between the anatase and rutile form of titania pigment can be seen. In general, the former adsorbs Tinuvin 770 more energetically and prolifically than the latter. This could be explained by the higher surface acidity of anatase particles, which can react with the amine functionalities of the Tinuvin 770. The Brønsted acidity of anatase bridged hydroxyls is sufficient for the protonation of the amine functionalities. The adsorption of the amines can also occur by hydrogen bond formation with surface hydroxyl species. However, according to this explanation, nanoparticle A, containing a higher OH content and featuring a larger N_2 BET surface area should adsorb the most energetically and

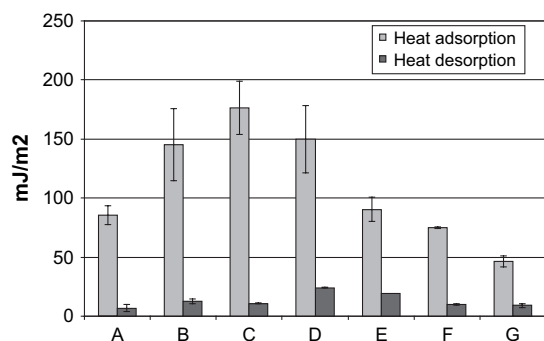


Fig. 5. Heat of adsorption and desorption (mJ m^{-2}) for Tinuvin 770 (adsorption data are all exothermic, the change of the energy has been reversed to facilitate comparison).

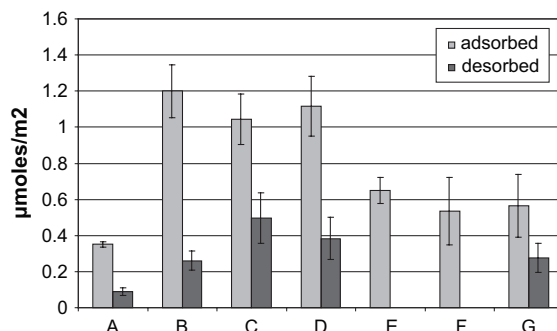


Fig. 6. Amount of Tinuvin 770 adsorbed and desorbed onto titanium dioxide particles.

prolifically than the rest of the pigments (see Fig. 7). Therefore, the adsorption and desorption behaviour of anatase particles is not related to surface area when particles are below a certain size. The larger particulate anatase (Samples B, C and D) showed sensibly similar absorption characteristics.

The low adsorption density displayed by pigment A may be related to the mode of adsorption of the stabiliser onto this pigment. The internal porosity of this pigment may not be accessible to the stabiliser molecule, thus a dramatic reduction in the adsorption density will then be observed. This feature can be observed in Figs. 8 and 9. The heat of adsorption and amount adsorbed versus the BET surface area for anatase particles have been plotted in order to explain this fact. It can be seen that as the potential surface area is increased the energy of adsorption and the amount of Tinuvin 770 adsorbed also increases. However, the linearity is not respected by pigment A.

Other factors reducing the adsorption activity of pigment A may be the adsorbed water. This pigment has not been subjected to a thermal treatment and thus the amount of water adsorbed in the lattice is higher than for the nanoparticles B, C and micron sized pigment D. Pigment A may be very much affected by this because it may contain molecular clusters of water in its pores.

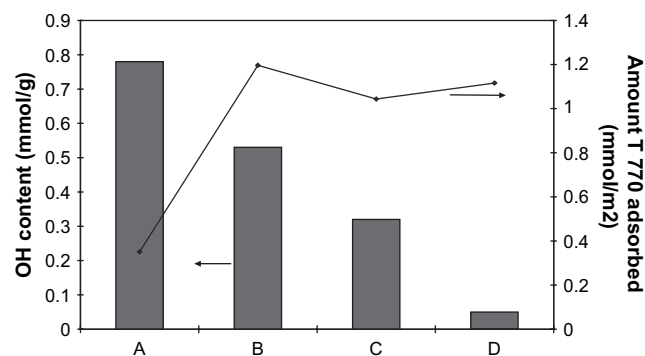


Fig. 7. Variation of OH content (mmol g^{-1}) and amount adsorbed for nanoparticles A, B, C and pigmentary D.

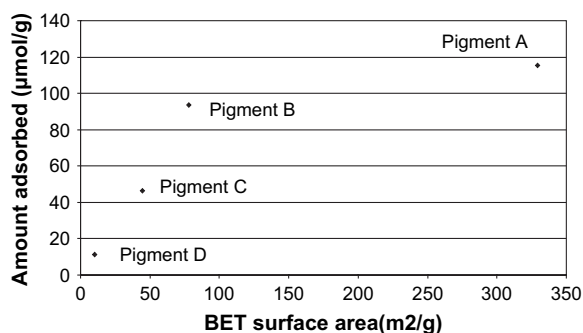


Fig. 8. Amount of Tinuvin 770 adsorbed ($\mu\text{mol g}^{-1}$) versus BET surface area for nanoparticles A, B, C and D.

Micron sized rutile particles showed little adsorption. It can be observed that the coating has an influence in the adsorption of the stabiliser onto the pigment. Pigment G in particular appeared to retain Tinuvin 770 less strongly than the other rutile pigments.

3.4. Adsorption of Irganox 1010

Fig. 10 shows the heat of adsorption and desorption of Irganox 1010 on seven different titanium dioxides. Here again, it can be seen that the energy released during adsorption is greater than that required for desorption. It can be observed here that anatase pigments adsorbed more energetically than the rutile pigments. The most energetic interaction took place on the intermediate particle size; pigment B followed by nanoparticle C and pigmentary D. Here again, nanoparticle A adsorbed less energetically than the rest of the pigments.

Fig. 11 compares the amount of Irganox 1010 adsorbed for the different titanium dioxide pigments. This data showed interesting and related trends. Here again, differences between the anatase and rutile form of titania can be seen. In general, the former adsorbs Irganox 1010 more energetically and prolifically than the latter. Moreover, the adsorption and desorption behaviour of anatase particles does not follow a pattern. The largest amount of Irganox 1010 was adsorbed on

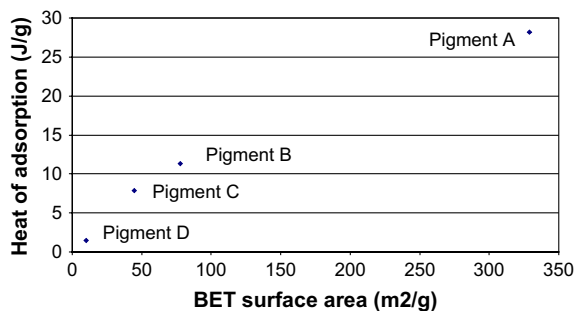


Fig. 9. Heat of adsorption (J g^{-1}) for Tinuvin 770 versus BET surface area for nanoparticles A, B, C and D.

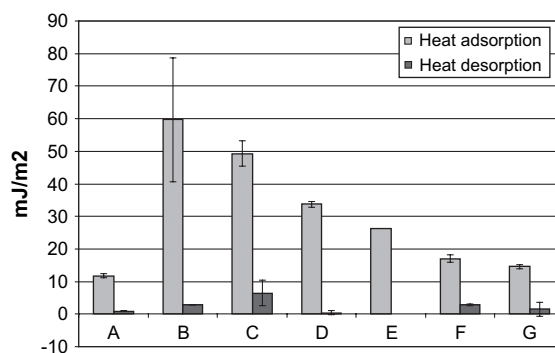


Fig. 10. Heat of adsorption and desorption (mJ m^{-2}) for Irganox 1010 (adsorption data are all exothermic, the change of the energy has been reversed to facilitate comparison).

micron sized titanium dioxide (D), followed by the nanosized particles C, B and A.

Figs. 12 and 13 show that for nanoanatase pigments B, C, and D there is a near-linear increase in heat of adsorption with increasing surface area. It is evident that Irganox 1010 could not penetrate the pore structure between the highly aggregated pigment A particles, as with Tinuvin 770 the adsorption may also have been blocked by adsorbed water. The bulkiness of the Irganox 1010 molecule may also hinder its adsorption, it may struggle to enter the interstices of aggregates of pigment B and C, thus explaining the reduced amount adsorbed.

Micron sized rutile particles showed less adsorption than the anatase pigments. It can be observed that the coating has a greater influence on the adsorption of the stabiliser onto the pigment. The heavily coated pigments F and G adsorbed less stabiliser than the slightly coated pigment E.

The FMC data highlight the differences in the energy of adsorption/desorption behaviour for the different stabilisers. The adsorption of Irganox 1010 onto pigments is much less energetic than that of Tinuvin 770 and is a reflection of the reduced interaction of the hindered phenolic hydroxyl group and the ester groups of Irganox 1010 with Ti–OH groups and associated

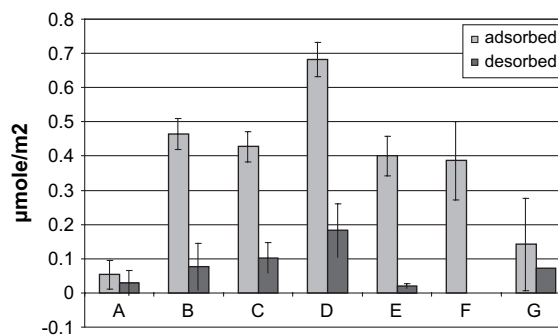


Fig. 11. Amount of Irganox 1010 adsorbed and desorbed on titania pigments.

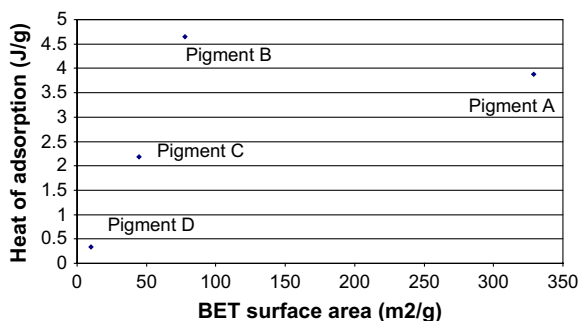


Fig. 12. Heat of adsorption (J g^{-1}) for Irganox 1010 versus BET surface area for nanoparticles A, B, C and D.

water relative to the much more basic piperidine amine groups of Tinuvin 770.

The other factor restricting strong adsorption in the case of Irganox 1010 is its sterically awkward shape and large size. The permanence of adsorption may however be due to multipoint adsorption. The other nanosized pigments (B and C) show significantly stronger adsorption of Irganox 1010 due to a change in morphology from substantially nano-porous to a much reduced porosity solid and a reduction in surface concentration of hydroxyl groups. The latter will tend to a reduction in the tendency to adsorb molecular water. This aspect will reduce adsorption activity due to the fact that the adsorbate molecule will need to overcome the existing hydrogen bonds if adsorption is to occur. The piperidinyl amine groups of Tinuvin 770 are of sufficient basicity to do this, the phenolic hydroxyl groups of Irganox 1010 are not.

3.5. Modelling

The structures of the stabilisers used in this study have been modelled using AccuModel (version 1.1). Figs. 14 and 15 show the geometry of Tinuvin 770 and Irganox 1010 after energy minimisation has been carried out. Molecular modelling has been used to represent and predict the structure of the molecules graphically and physically. Although it helps to visualise molecules,

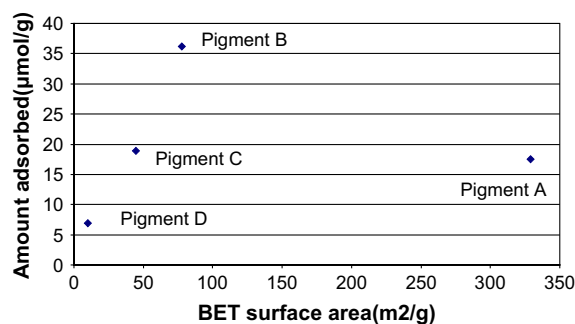


Fig. 13. Amount of Irganox 1010 adsorbed ($\mu\text{mol g}^{-1}$) versus BET surface area for nanoparticles A, B, C and D.

it should be borne in mind that it is a model and does not always provide an accurate representation but a simulation.

The energy minimisation procedure is carried out to minimise the energy of the structure imputed, the sequence begins with the drawn geometry where the initial energy calculation begins. The Cartesian coordinates of the atom of the molecule are modified so that the energy of the system decreases and this is carried out until a minimum energy has been reached and is known as the potential energy surface. The minimum energy arrangements of the atoms correspond to the stable phases of a system; movement away from the minimum gives a configuration with a higher energy.

The molecular model for Irganox 1010 shows that there is possibly more scope for interaction via the esters group than via phenolic hydroxyl groups, which appears somewhat hindered by the *t*-butyl groups. FMC studies conducted within the research group on the adsorption of Irganox 1010 onto silica showed that adsorption can occur via the phenolic hydroxyl group and the ester group [2]. It may be envisaged however that the acidity of Ti–OH may be less than that of Si–OH.

Tinuvin 770 is much simpler molecule than Irganox 1010. The ester groups at each end of the molecule appear exposed and together where the relative flatness of the alkyl chain may favour two point “flat” adsorption of Tinuvin 770. Vertical adsorption via the piperidinyl amine group may also occur.

Regarding the structures of each stabiliser, it can be observed that Irganox 1010 is more packed, where the *t*-butyl groups hinder the possibility of hydroxyl groups to react with the titania pigment. Also the carboxyl groups of this molecule are hindered by the phenol molecule, being more difficult to react with the pigment.

3.6. DRIFTS analysis

Since physical–chemical interactions are believed to be involved, infrared analysis was also carried out. The mode of adsorption of the stabilisers is apparent from the DRIFTS data with examples shown in Figs. 16 and 17. DRIFTS analysis on the titanium dioxide treated in the FMC affords some insight into the manner in which additives adsorb. The significant bands of Irganox 1010 (Fig. 16) are OH stretching (3627 cm^{-1}), CH stretching centred at 2900 cm^{-1} , carbonyl stretching (1745 cm^{-1}) methylene CH deformation (1440 cm^{-1}) and methyl CH deformation (1360 cm^{-1}). For all the seven pigments treated with Irganox 1010 in the FMC cell, the following spectral perturbations are apparent. The ester carbonyl group is broadened and shifted to lower energy relative when the additive is unbound. Decrease in the intensities and shift of the C–O stretching bands (1240 and 1090 cm^{-1}). The OH stretch (3627 cm^{-1}) of the Irganox 1010 is also reduced in relative intensity.

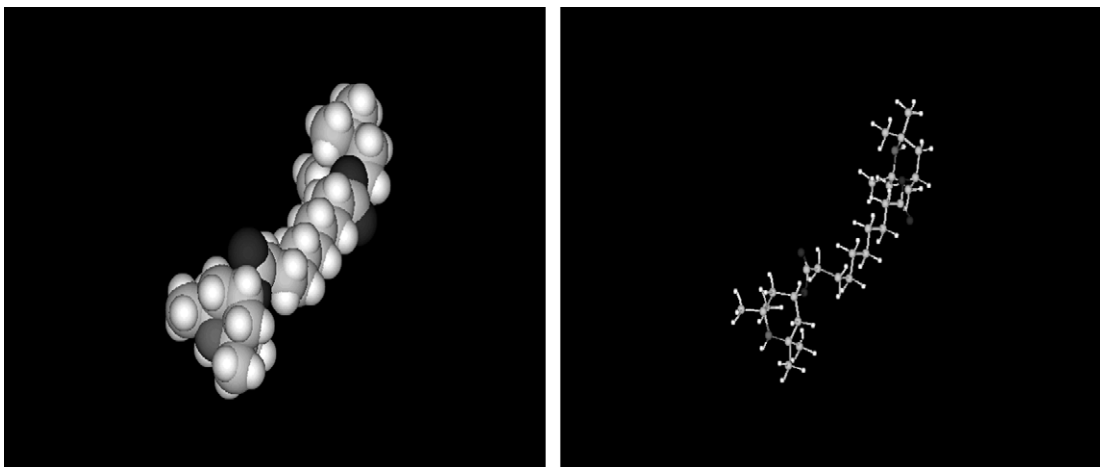


Fig. 14. Energy minimised molecular structures of Tinuvin 770.

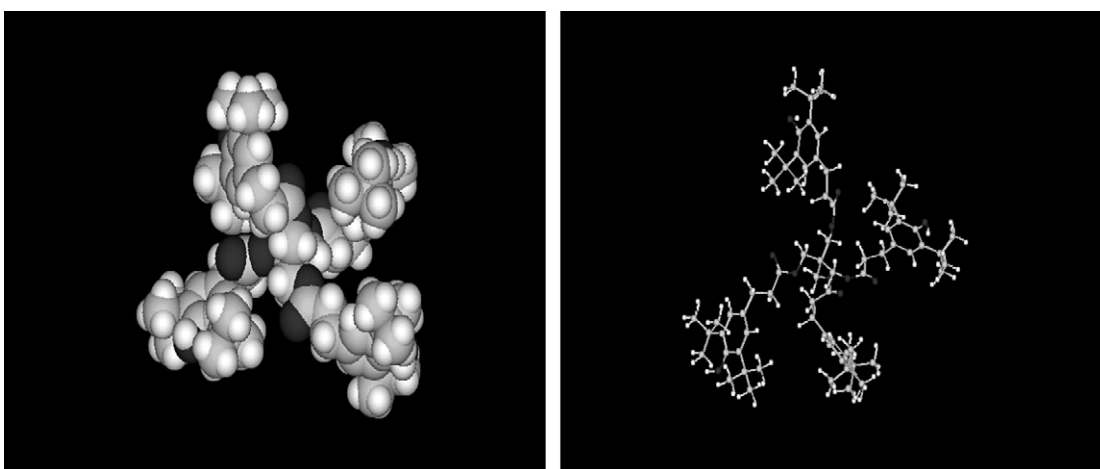


Fig. 15. Energy minimised molecular structures of Irganox 1010.

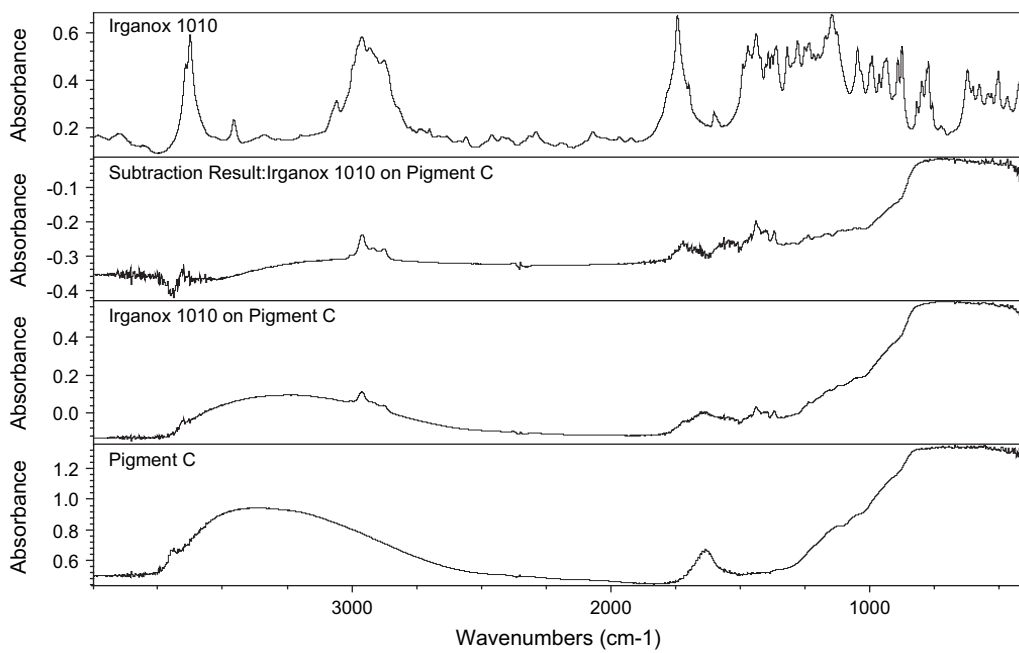


Fig. 16. DRIFTS spectra of Irganox 1010, pigment B and the sample extracted from the FMC cell after the adsorption/desorption process had taken place.

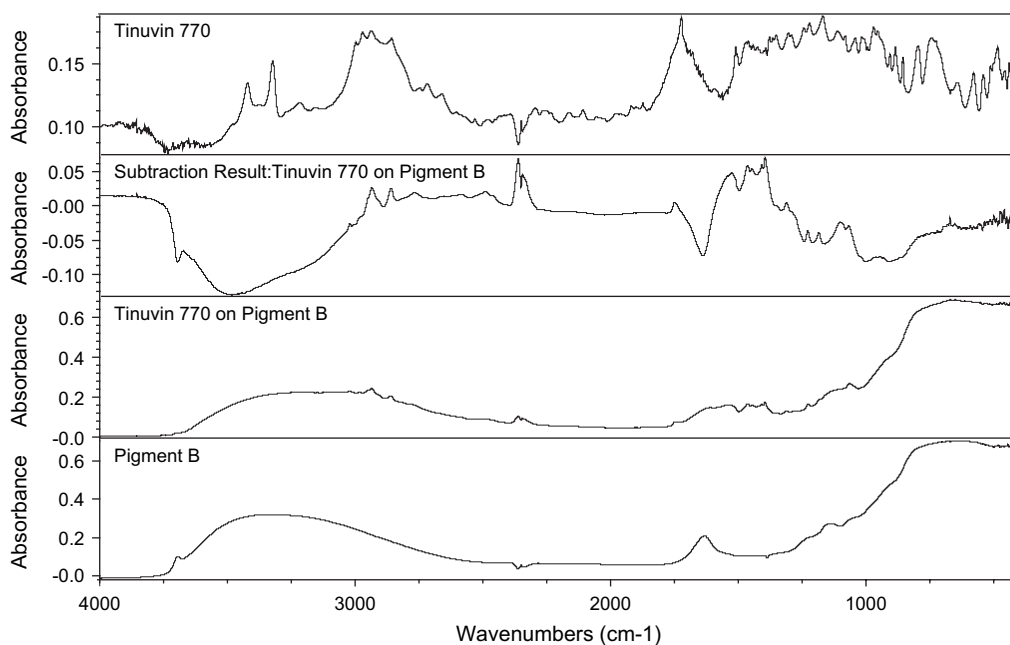


Fig. 17. DRIFTS spectra of Tinuvin 770, pigment B and the sample extracted from the FMC cell after the adsorption/desorption process had taken place.

These observations clearly reflect adsorption via the ester group and phenolic OH groups.

Similar observations are also apparent for Tinuvin 770 (Fig. 17) where a reduction in the NH stretching intensity was observed thereby indicating adsorption via the substituted piperidine portion of the molecules.

4. Conclusions

Model system studies based on 2-propanol oxidation and hydroxyl analysis go some way towards predicting titania photoactivities. The increase in the hydroxyl content with the surface area is related to an enhancement in the photoactivity of the particles. Clear trends cannot be observed due to the amorphous character of the uncalcined pigment which introduces impurities for trapping electrons and holes altering the photoactivity of the pigment. The porous structure of this particular pigment also hampers the access of the reactants differing in the photoactivities with the rest of the pigments. Adsorption studies onto the pigments were undertaken by the flow microcalorimetry technique. These showed that the calcined crystalline anatase particles adsorbed more energetically and prolifically than rutile pigments. The uncalcined amorphous nanoanatase showed very weak adsorption of Irganox 1010 and Tinuvin 770 due to the highly conglomerated nature of the pigment particles and the high level of surface water that may also be bridging the primary particles, this water is retained strongly on the surface by the Ti–OH groups.

Calcinations of this amorphous nanoanatase yielded less aggregated crystalline particles with a lower surface water content due to reduced surface concentration of Ti–OH groups. This led to significantly increased adsorption of Tinuvin 770 and Irganox 1010. Due to the sterically awkward shape of Irganox 1010 and highly hindered phenolic OH groups, this molecule adsorbed less strongly than Tinuvin 770. The micron sized rutile pigments adsorbed the two stabilisers somewhat less strongly than the anatase samples while coating of the rutile with alumina also tended to reduce adsorption activity.

References

- [1] Wolfschewenger J, Hauer A, Gahleitner MG, Neibl W. In: *Proceedings Eurofillers 97*. Manchester, UK: British Plastics federation; 1997. p. 375–77.
- [2] Liauw CM, Childs A, Allen NS, Edge M, Franklin KR, Collopy DG. *Polym Degrad Stab* 1999;65:207.
- [3] Fowkes FM. Acid–base interactions. In: Mittal KL, Anderson Jr HR, editors. *VPS*; 1991. p. 93–115.
- [4] Ashton DP, Briggs D. Particulate filled polymer composites. In: Rothon RN, editor. *Analytical technique for characterising filler surfaces*. Harlow: Longman Scientific and General; 1995. p. 90–105.
- [5] Pena JM, Allen NS, Edge M, Liauw CM, Noiset O, Valange B, et al. *J Mater Sci* 2001;36:2885–98.
- [6] Pena JM, Allen NS, Edge M, Liauw CM, Noiset O, Valange B. *J Mater Sci* 2001;36:4419–31.
- [7] Pena JM, Allen NS, Edge M, Liauw CM, Noiset O, Valange B, et al. *J Mater Sci* 2001;36:4443–57.

- [8] Allen NS, Edge M, Ortega A, Liauw CM, Verran J, Stratton J, et al. *Polym Degrad Stab* 2004;85:927–46.
- [9] Allen NS, Edge M, Ortega A, Liauw CM, Stratton J, McIntyre RB. *Polym Degrad Stab* 2002;78:467–78.
- [10] Broonstra AH, Mutsears CAHA. *J Phys Chem* 1975;79(16):1694.
- [11] Hague DC, Mayo MJ. *J Am Ceram Soc* 1994;77:1957.
- [12] Hong S, Lee M, Hwang H, Lim K, Park S, Ju C, et al. *Sol Energ Mater Sol Cell* 2003;80:273.
- [13] Wang YM, Liu SW, Lu MK, Wang SF, Gu FX, Gai Z, et al. *J Mol Catal A Chem* 2004;215:137.
- [14] Rothenberger G, Moser J, Gratzel M. *J Am Chem Soc* 1985;107:8054.